ISSN 1087-6596, Glass Physics and Chemistry, 2006, Vol. 32, No. 1, pp. 99–105. © Pleiades Publishing, Inc., 2006.
Original Russian Text © A.E. Galashev, V.A. Polukhin, I.A. Izmodenov, O.R. Rakhmanova, 2006, published in Fizika i Khimiya Stekla.

Simulation of Noncrystalline Silicon Nanoparticles: A Computer Experiment

A. E. Galashev*, V. A. Polukhin, I. A. Izmodenov***, and O. R. Rakhmanova*****

* *Institute of Thermal Physics, Ural Division, Russian Academy of Sciences, ul. Amundsena 106, GSP-828, Yekaterinburg, 620219 Russia*

** *Institute of Metallurgy, Ural Division, Russian Academy of Sciences, ul. Amundsena 101, GSP-828, Yekaterinburg, 620219 Russia*

*** *Institute of Industrial Ecology, Ural Division, Russian Academy of Sciences, ul. S. Kovalevskoi 20a, GSP-594, Yekaterinburg, 620219 Russia*

Received January 13, 2005

Abstract—The physical properties of vitreous and amorphous silicon nanoparticles containing 300, 400, and 500 atoms are investigated by the molecular dynamics method. For a limited number of degrees of freedom, the internal energy of the amorphous phase is often less than the internal energy of the vitreous phase. The structure of the central region of silicon nanoparticles is studied in detail by constructing Voronoi polyhedra, which make it possible to determine the mean length of bonds and their number. The differences between the structures of nanoparticles in the amorphous and vitreous states are determined by the differences in the distribution of angles between Si–Si bonds and the distribution of bond lengths. Local arrangements of atoms in vitreous silicon nanoparticles are characterized by larger variations in the interatomic distances. The self-diffusion coefficients determined from mean-square atomic displacements are smaller for amorphous nanoparticles due to dominant diffusion over dangling Si–Si bonds.

DOI: 10.1134/S1087659606010135

INTRODUCTION

The structure of solid clusters formed by several tens of atoms every so often does not correspond to the crystal lattice of a bulk solid [1]. Silicon clusters containing of the order of twenty atoms have a large number of isomers and are characterized by a wide variety of atomic arrangements [2]. A spherical shape of silicon clusters is considered equilibrium when clusters involve more than 28 atoms [3]. *Ab initio* calculations were performed in order to reveal sizes at which silicon clusters transform into a diamond-like structure [4]. It was demonstrated that the structure of clusters containing 100 and more atoms can transform into a bulk structure. However, when hydrogen is adsorbed on the surface of silicon clusters, smaller sized clusters have a tendency toward formation of the bulk diamond structure due to the saturation of dangling bonds [5].

Hereafter, for definiteness, the solid state formed not from a liquid (i.e., not by quenching a melt) will be referred to as the amorphous state. The glass will be considered to mean a nonequilibrium solid state formed through rapid supercooling of the liquid. According to [6, 7], this system undergoes amorphous–liquid and liquid–liquid first-order transitions. However, molecular dynamics simulations with the use of the Stillinger–Weber potential revealed only one (liquid–liquid) transition at 1060 K [8–10]. There are many works devoted to investigations into the properties of bulk silicon [11–14] and small-sized clusters consisting of silicon atoms whose number does not exceed 50 [15–17]. The physical properties of silicon clusters containing from 30 to 480 atoms were studied by Zachariah *et al.* [18]. It was found that, over a wide range of temperatures (600 K < T < 2000 K), the structure of clusters corresponds to the structure of vitreous silicon.

The purpose of this work was to simulate amorphous and vitreous silicon particles within the molecular dynamics model and to reveal the differences between the energies, structures, and kinetic properties of nanoparticles in the vitreous and amorphous states.

THE STILLINGER–WEBER POTENTIAL

The interatomic interaction potential Φ proposed by Stillinger and Weber [19] consists of two terms, so that the potential energy U can be represented in the form

$$U = \varepsilon A\left[\sum_{(i,j)}\Phi_{ij}^{(2)}(r_{ij}) + \frac{\lambda}{A}\sum_{(jik)}\Phi_{jik}^{(3)}(r_{ij}, r_{ik})\right], \qquad (1)$$

where the parameter εA is the energy at which the required covalent bonding is attended in a dynamic system. This energy ensures realistic stretching vibrations of atoms. The parameter A in relationship (1) fulfils an auxiliary function providing the satisfaction of the con-

Parameters of the Stillinger–Weber potential

Parameter	Crystalline or liquid silicon	Amorphous state of bulk silicon
ε, eV	2.16826	1.64833
A	7.049556277	7.049556277
B	0.6022245584	0.6022245584
σ, nm	0.20951	0.20951
p	4	4
a	1.8	1.8
λ	21.0	31.5
γ	1.2	1.2

dition $A\Phi_{ij}^{(2)}(r_{ij}^{\min}) = -1$ for the pair potential at the minimum.

The contribution of pair interactions to the potential Φ is defined as

$$\Phi_{ij}^{(2)}(r_{ij}) = \left[B\left(\frac{r_{ij}}{\sigma}\right)^{-p} - 1\right]\exp\left(\frac{1}{r_{ij}/\sigma - a}\right)\Theta(a - r_{ij}/\sigma), \quad (2)$$

and the contribution of three-particle interactions is written in the form

$$\Phi_{jik}^{(3)}(r_{ij}, r_{ik}) = \exp\left[\frac{\gamma}{r_{ij}/\sigma - a} + \frac{\gamma}{r_{ik}/\sigma - a}\right] \times (\cos\theta_{jik} - \cos\theta^0)^2\Theta(a - r_{ij}/\sigma)\Theta(a - r_{ik}/\sigma). \quad (3)$$

Here, a, B, p, and γ are empirical parameters; $\Theta(x)$ is the Heaviside step function; and θ^0 is the tetrahedral angle ($\cos\theta^0 = -1/3$). The intensity of bending vibrations is defined by the quantity ελ. Atomic displacements responsible for the change in the bond angle are predominantly associated with the three-particle interactions. The parameters used are listed in the table. The chosen parameter σ provides the fulfillment of the equality $A\Phi_{ij}^{(2)}(2^{1/6}) = 0$. The parameters listed in the second column of the table were obtained with the use of experimental data for crystalline and liquid silicon. The potential parameters in the third column of the table served for simulating the bulk amorphous phase of silicon [20]. These parameters were determined by fitting the calculated values of the bulk modulus, Poisson ratio, velocity of sound, and density to the experimental data.

COMPUTATIONAL MODEL

Numerical integration of the equations of motion was performed using the Verlet algorithm [21], which includes the direct calculations of particle velocities. This algorithm is one of the most stable algorithms, on the one hand, and makes it possible to control the temperature in the model with a sufficient accuracy, on the other hand. The time step Δt was equal to 10^{-16} s. The calculations were carried out for the systems containing 300, 400, and 500 Si atoms. At each nanoparticle size, the disordered solid state was simulated in two different ways. In the first case, a nanoparticle in the initial state had a crystal structure with a diamond-like lattice, i.e., a structure of bulk crystalline silicon. The vitreous state was simulated as follows. At the first stage of calculations, the crystalline nanoparticle was held at a temperature of 3000 K for 1000000 time steps. In this time interval, the nanocrystal melted and acquired a structure of the liquid nanoparticle. Then, the system was rapidly cooled in the course of the next 1000000 time steps. The cooling rate was approximately equal to 0.0027 K/step, i.e., approximately 2.7×10^{13} K/s. Toward the end of this stage of calculations, the nanoparticle temperature was 300 ± 50 K. Thereafter, the structural relaxation of the rapidly cooled nonequilibrium nanoparticle was simulated for 1000000 time steps at a temperature of 300 K. As a result, we obtained the system in the vitreous state with a limited number of degrees of freedom. The amorphous state of nanoparticles was simulated in another way. Preliminarily, a configuration with a loose irregular atomic arrangement, in which the distances between each Si atom and geometric neighbors did not exceed 0.3 nm, was produced by a random-number generator in a spherical region of the corresponding size. The relaxation of this structure was performed in two stages at a temperature of 300 K. The first stage involved 10000 time steps Δt. At this stage, the interaction between Si atoms was described by the Stillinger–Weber potential with the parameters used for simulating the bulk amorphous phase of silicon [19] (see the table). The calculations led to a considerable decrease in the nanoparticle volume and interatomic distances. The time of these calculations was limited in order to avoid the atomic overlap determined by comparing the interatomic distances with the parameter σ. The Stillinger–Weber potential with the parameters proposed for simulating bulk amorphous silicon appeared to be inappropriate for simulating amorphous Si nanoparticles. When the properties of the Si nanoparticle were calculated by the molecular dynamics method for a few tens of thousands of time steps with the potential parameters given in the third column of the table, Si atoms coalesced in the system. In a rough approximation, these calculations can be treated as the simulation of forming the silicon nanoparticle in a noble-gas medium when collisions of gas molecules with Si atoms lead to the formation of the nanoparticle. The amorphous state of nanoparticles was also simulated using the Stillinger–Weber potential with the parameters from the second column of the table, i.e., the parameters proposed by Vink *et al.* [20]. The relaxation of the obtained amorphous state was carried out for 1000000 time steps. The configurations of the Si_{300} nanoparticle in the vitreous and amorphous states are depicted in Fig. 1. It can be seen from this fig-

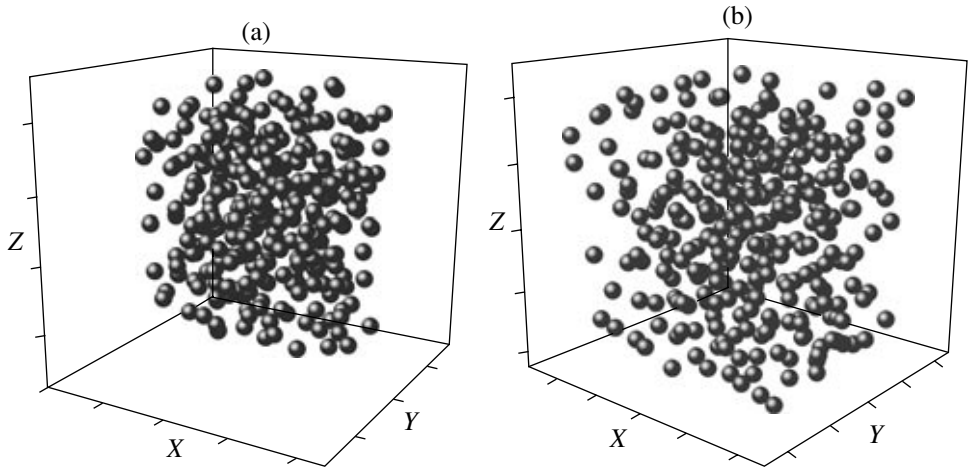

Fig. 1. Configurations of the Si_{300} nanoparticle in the (a) vitreous and (b) amorphous states. Instant of time, 100 ps; $T = 300$ K.

ure that the vitreous nanoparticle, especially in the central region, is characterized by a closer packing. The surface atoms of the vitreous particle form a loose layer. The amorphous nanoparticle has a different structure with a looser atomic packing. The central region is inhomogeneous and contains close-packed fragments and holes that are absent in the structure of the vitreous nanoparticle.

The structure of larger sized particles reflects the main features of the structure of the Si_{300} nanoparticles. Figure 2 shows the densities of spherical concentric layers of the vitreous (curve *1*) and amorphous (curve *2*) Si_{500} nanoparticles. The mean density of the vitreous nanoparticle (Fig. 2, straight line *3*) is higher than that of the amorphous nanoparticle (Fig. 2, straight line *4*) but is lower than the density of the crystal (Fig. 2, straight line *5*). The density in the central region of the vitreous Si_{500} nanoparticle is higher than that of the corresponding amorphous particle. The changeover from the packing with a high density to the packing with a low density is not so sharp as for the amorphous nanoparticle. On the whole, the amorphous nanoparticle is characterized by a more uniform density distribution and has a thinner surface layer with the density lower than the mean density.

INTERNAL ENERGY

The time dependences of the internal energy U for the vitreous and amorphous nanoparticles are shown in Fig. 3. After quenching ($t = 0$), the internal energies differ substantially depending on the nanoparticle size. At this instant of time, the Si_{300} and Si_{400} nanoparticles have the lowest and highest internal energies, respectively. However, even within 50 ps, the internal energies of the nanoparticles become close to each other and the structural relaxation of the vitreous state, for the most part, is completed. Subsequently, the internal energies U fluctuate with respect to their quasi-equilibrium values. At the end of calculations, the Si_{500} and Si_{400} vitreous nanoparticles have the lowest and highest internal energies, respectively. Note that the internal energy of the Si_{500} nanoparticle (–3.75 eV) is close to the internal energy calculated for the Si_{480} particle by Zachariah *et al.* [18] at $T = 600$ K with the use of the Stillinger–Weber interaction potential. The inset to Fig. 3 shows the behavior of the internal energy during the simulation of the amorphous state. In this case, the nanoparticle state obtained after short calculations that simulate the condensation of silicon atoms in a noble gas is taken as the state at the initial instant of time. The calculations whose data are presented in the inset to Fig. 3 can be considered the simulation of the condensation of Si atoms in vacuum at a considerably lower rate. The internal energy of the system at this stage depends strongly on the number of atoms contained in the nanoparticle. For the Si_{300} nanoparticle, the internal energy

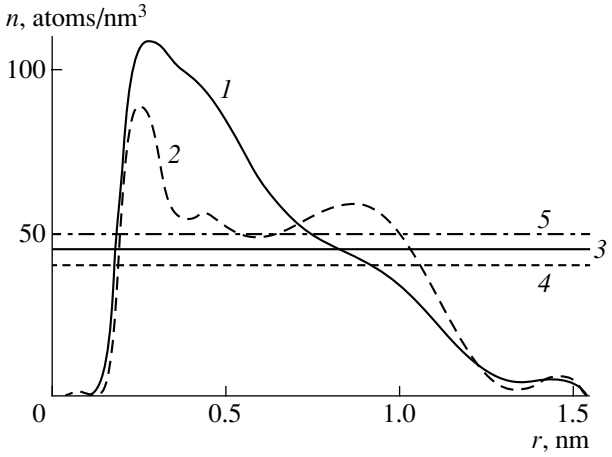

Fig. 2. Radial atomic density distributions for the (*1*) vitreous and (*2*) amorphous Si_{500} nanoparticles, mean densities of the (*3*) vitreous and (*4*) amorphous Si_{500} nanoparticles, and (*5*) the density of crystalline silicon.

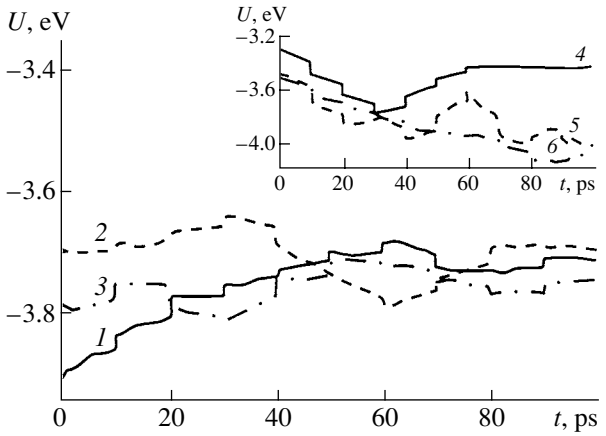

Fig. 3. Time dependences of the internal energy of the (*1*, *4*) Si_{300}, (*2*, *5*) Si_{400}, and (*3*, *6*) Si_{500} silicon nanoparticles in the (*1–3*) vitreous and (*4–6*) amorphous states.

U initially decreases, then (beginning with t = 30 ps) increases to U = –3.4 eV, and remains unchanged at times longer than t = 60 ps. The internal energy of the Si_{400} nanoparticle decreases with strong fluctuations in time. The internal energy of the Si_{500} nanoparticle decreases more smoothly. The final energy U for the nanoparticles in the amorphous state, as a rule, is lower than that for the nanoparticles in the vitreous state. The exception is provided by the Si_{300} nanoparticle whose energy in the amorphous state is higher than that in the vitreous state.

STRUCTURE OF NANOPARTICLES

Structural transformations at different stages of simulation can be traced from a change in the distribution of bond angles φ. The bond angle is considered to mean an angle whose vertex is located at the center of one of the Si atoms and whose sides (Si–Si segments) do not exceed 0.3 nm. This distance is close to the length parameter in the flexible Morse potential describing the Si–Si interaction [22]. The distributions of angles φ that characterize the states of the Si_{300} nanoparticle at different stages of simulation are depicted in Fig. 4. At the first three stages of calculations performed in order to simulate the vitreous state, the main maximum in the distributions of angles φ is observed at 60°. At T = 3000 K (first stage), there appears a peak at φ = 114° in the distribution of angles φ. Note that the angle φ = 109.5° corresponds to the tetrahedral coordination of atoms. Rapid cooling (second stage) is accompanied by an increase in the height of the peak at an angle of 108°.

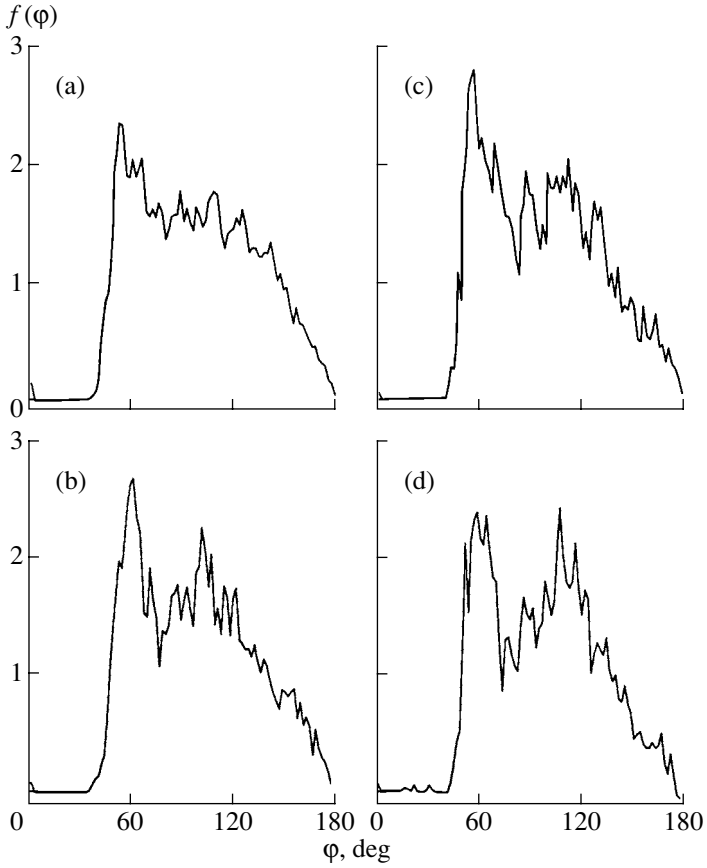

Fig. 4. Distributions of angles φ between Si–Si bonds in the Si_{300} nanoparticle (a) during melting of the crystalline nanoparticle, (b) in the course of quenching, and in the (c) vitreous and (d) amorphous states.

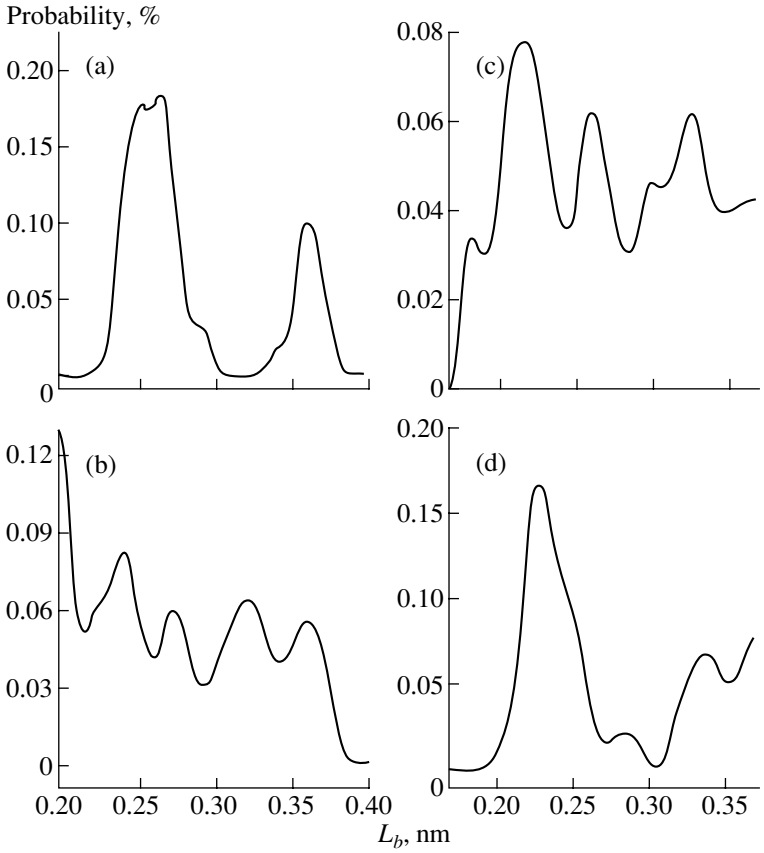

Fig. 5. Distributions of distances between the nearest geometric neighbors in the Si_{500} nanoparticle (a) during melting of the crystalline nanoparticle, (b) in the course of quenching, and in the (c) vitreous and (d) amorphous states.

During the relaxation of the glass structure (third stage), there arise a broad peak in the vicinity of the angle $\varphi = 114°$ (with a sharp maximum at 117°) and a pronounced peak at $\varphi = 102°$. The amorphous state of the nanoparticle (fourth stage) is characterized by a considerable increase in the intensity of the distribution of angles φ in the angle range that corresponds to the coordination of atoms in the diamond lattice with a sharp maximum at $\varphi = 108°$. In this case, the peaks at angles of 60° and 108° are comparable in intensity.

The Si–Si bond lengths in the nanoparticles were determined by constructing Voronoi polyhedra. The faces of Voronoi polyhedra determine the nearest geometric neighbors. The mean distance to the nearest neighbors within the interaction range ($R \le 0.37$ nm) was taken as the Si–Si bond length L_b. The distributions of Si–Si bond lengths thus obtained in the Si_{500} nanoparticle at different stages of simulation are shown in Fig. 5. At $T = 3000$ K, the distribution of bond lengths L_b has a bimodal form. In the silicon melt, there are two specific distances that characterize the mutual arrangement of neighbors, namely, in dense local groupings and between atoms of adjacent groupings. During rapid cooling of the system, there appear five maxima with the main maximum at $L_b = 0.2$ nm in the distribution of bond lengths L_b. Most likely, this stage is attended by the formation of many types of groupings with different atomic arrangement. Upon relaxation of the quenched state (Fig. 4c), the number of peaks in the distribution of bond lengths L_b decreases to three. The most intense peak is shifted toward the right; i.e., the distances in dense local groupings somewhat increase. In the amorphous state, the distribution of bond lengths L_b in the nanoparticles exhibits two peaks: a dominant peak and a split peak with a relatively low intensity. The former peak associated with the dense local groupings of atoms is located at a somewhat larger distance as compared to the corresponding peak in the distribution of bond lengths L_b in the Si_{500} vitreous nanoparticle. The difference between the distributions of bond lengths L_b for the nanoparticles in the vitreous and amorphous states suggests that their structures differ substantially.

THE SELF-DIFFUSION COEFFICIENT

The velocity autocorrelation functions for the Si_{400} nanoparticle in the vitreous and amorphous states are depicted in Fig. 6a. The velocity autocorrelation function for the Si_{400} vitreous nanoparticle decreases monotonically with time. However, this function does not completely decay for 20 ps. In vitreous silicon nanoparticles with the close packing and covalent bonding, atomic velocities turn out to be strongly correlated in time and slowly change their direction. As a conse-

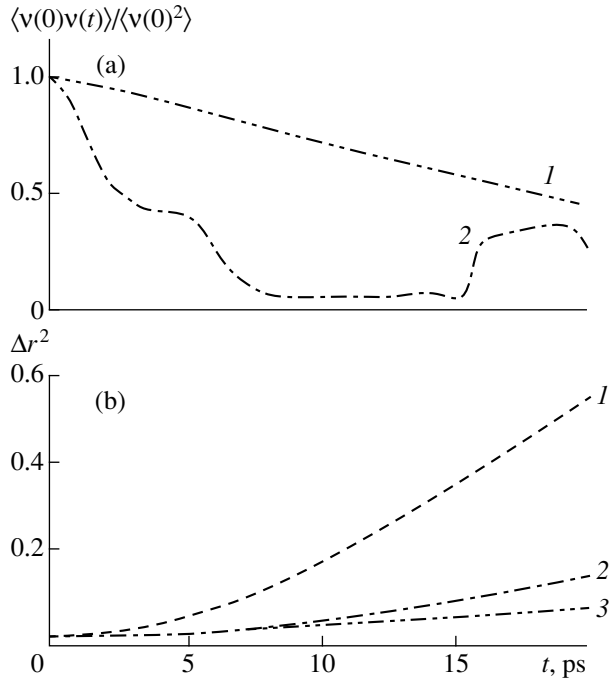

Fig. 6. (a) Velocity autocorrelation functions for the Si_{400} nanoparticle in the (*1*) vitreous and (*2*) amorphous states and (b) mean-square atomic displacements in the Si_{400} nanoparticle (*1*) in the course of quenching and in the (*2*) vitreous and (*3*) amorphous states.

quence, the velocity autocorrelation function decays slowly. Since the vitreous silicon particles have structures with low-coordination short-range order and rigid covalent bonds, the translational motion of atoms occurs through trajectories with characteristic tangential portions and orbital bending around centers with the strongest bonds [23]. The situation changes drastically in the case of the amorphous state. A looser packing and the presence of holes provide considerably faster switching of Si bonds. This favors a more rapid decay of the velocity autocorrelation function. However, in this case, too, the velocity autocorrelation function does not intersect the abscissa axis, i.e., does not take on negative values. The self-diffusion coefficients cannot be determined from this function. The time dependences of the mean-square atomic displacement $\langle \Delta r^2 \rangle(t)$ for the Si_{400} nanoparticle in the course of rapid cooling and structural relaxation to the vitreous state and also for this nanoparticle in the amorphous state are depicted in Fig. 6b. It can be seen from Fig. 6b that the largest atomic displacements are observed in the course of quenching (rapid cooling). The mean atomic displacements in the vitreous nanoparticles are always larger than those in the amorphous nanoparticles. The self-diffusion coefficients of atoms were determined from the relationship

$$D = \lim_{t \to \infty} \frac{\langle \Delta r^2 \rangle}{6t}, \quad (4)$$

where t is the time interval in which the displacement occurs. The self-diffusion coefficients of atoms in the vitreous silicon nanoparticles at 300 K are equal to $(0.109 \pm 0.001) \times 10^{-10}$ m²/s. The self-diffusion coefficients D for the amorphous silicon nanoparticles fall in the range $(0.054–0.097) \times 10^{-10}$ m²/s. The experimental diffusion coefficient in a surface region of silicon at T = 1273 K is equal to 0.04×10^{-10} m²/s [18], i.e., is approximately 2.7 times smaller than that for the amorphous nanoparticles studied in our work. However, our self-diffusion coefficients D are in good agreement with the self-diffusion coefficient (0.203×10^{-10} m²/s, T = 600 K) calculated for the Si_{480} vitreous particle in [18] with the use of the Stillinger–Weber potential. Note that, according to Zachariah *et al.* [18], the Stillinger–Weber potential underestimates the binding energy in bulk silicon; as a result, the computer experiment leads to an overestimated value of the surface diffusion coefficient. It should also be noted that the tight-binding molecular dynamics simulation of bulk silicon [24] also predicts the self-diffusion coefficients D larger than those obtained in experiments. In real physical experiments, it is difficult to eliminate surface oxidation that decreases the self-diffusion coefficient.

CONCLUSIONS

Covalent interactions govern specific properties of silicon, such as a high permittivity, a change in the sign of the temperature coefficient of thermal expansion at T = 120 K, etc. The transformation of materials into an ultradispersed state leads to a qualitative change in their properties. The nanoparticle sizes are frequently comparable to a characteristic scale of a physical phenomenon. In the majority of cases, unusual properties of nanomaterials manifest themselves when nanoparticle sizes become less than 100 nm. The characteristic size of the silicon nanoparticles under investigation is approximately equal to 3–3.5 nm. A large number of bonds in these nanoparticles are shorter than covalent bonds in silicon crystals. As is known, the presence of short bonds favors the metallization of silicon states. A decrease in the mobility of silicon atoms leads to an increase in the degree of bond covalency and is responsible for the crossover from a metallic behavior to a semiconducting behavior. The performed calculations demonstrated that bonds in vitreous and amorphous silicon nanoparticles differ radically from a diamond-like tetrahedral network of bonds. In this case, there is a clear tendency to the formation of angles between adjacent bonds that differ from an angle of 109.5°. In the structures of nanoparticles in both the vitreous and amorphous states, bonds form the angle $\varphi = 60°$, to a considerable extent, due to the irregular atomic packing. However, the second peaks in the distributions of bond angles φ in the vitreous and amorphous nanoparticles are observed at different angles. Compared to the amorphous silicon particle, the vitreous silicon nanoparticle is characterized by the distribution of bond

angles φ in which the location of the second peak is closer to a bond angle of 109.5°.

When studying differences between the physical properties of vitreous and amorphous silicon nanoparticles, important information can be obtained by calculating the self-diffusion coefficients. The largest self-diffusion coefficients were derived for the vitreous silicon nanoparticles, which have a dense atomic packing in the central region and a loose packing at the periphery. The amorphous silicon nanoparticles with a more uniform density distribution in the radial direction possess smaller self-diffusion coefficients. Possibly, this is associated with the fact that diffusion in nanoparticles occurs over Si–Si dangling bonds whose number in the vitreous silicon nanoparticles, as a rule, is larger than the number of dangling bonds in the amorphous silicon nanoparticles. Therefore, the amorphous silicon nanoparticles characterized by smaller self-diffusion coefficients preferably acquire semiconductor properties as compared to the vitreous silicon nanoparticles. An increase in the density of dangling bonds allows one to identify more reliably structural defects. In this case, the diffusion process in noncrystalline silicon particles can be treated as the formation, interaction, and migration of defects. In a number of cases, diffusion can proceed through the mechanism of relay-race switching of dangling bonds.

ACKNOWLEDGMENTS

This work was supported by the Russian Foundation for Basic Research (project no. 04-03-32053) and the Presidium of the Ural Division of the Russian Academy of Sciences within the Integration Project of the Ural Division–Far East Division of the Russian Academy of Sciences.

REFERENCES

1. Galashev, A.E., Stability of Single Vacancies and Multiple Vacancies in a Nickel Nanoparticle, *Poverkhnost,* 2005, no. 1, pp. 77–84.
2. Kawazoe, Y., Kondow, T., and Ohno, K., *Clusters and Nanomaterials: Theory and Experiment*, Berlin: Springer-Verlag, 2002.
3. Kaxiras, E. and Jackson, K., Shape of Small Silicon Clusters, *Phys. Rev. Lett.*, 1993, vol. 71, no. 5, pp. 727–730.
4. Ohno, K., Esfarjani, K., and Kawazoe, Y., *Computational Materials Science: From Ab Initio to Monte Carlo Methods*, Berlin: Springer-Verlag, 1999.
5. Polukhin, V.A., *Modelirovanie nanostruktury i prekursornykh sostoyanii* (Simulation of Nanostructures and Precursor States), Yekaterinburg: Ural. Otd. Ross. Akad. Nauk, 2004.
6. Ramakrishna, M.V. and Pan, J., Chemical Reactions of Silicon Clusters, *J. Chem. Phys.,* 1994, vol. 101, no. 9, pp. 8108–8118.
7. Donovan, E.P., Spaepen, F., Turnbull, D., *et al.*, Calorimetric Studies of Crystallization and Relaxation of Amorphous Si and Ge Prepared by Ion Implantation, *J. Appl. Phys.,* 1985, vol. 57, no. 7, pp. 1795–1804.
8. Keblinski, P., Bazant, M.Z., Dash, R.K., *et al.*, Thermodynamic Behavior of a Model Covalent Material Described by the Environment-Dependent Interatomic Potential, *Phys. Rev. B: Condens. Matter*, 2002, vol. 66, no. 6, pp. 4101–4118.
9. Broughton, J.Q. and Li, X.P., Phase Diagram of Silicon by Molecular Dynamics, *Phys. Rev. B: Condens. Matter*, 1987, vol. 35, no. 17, pp. 9120–9127.
10. Luedtke, W.D. and Landman, U., Preparation, Structure, Dynamics, and Energetic of Amorphous Silicon: A Molecular Dynamics Study, *Phys. Rev. B: Condens. Matter*, 1989, vol. 40, no. 2, pp. 1164–1174.
11. Sastry, S. and Angell, C.A., Liquid–Liquid Phase Transition in Supercooled Silicon, *Nature Mater.*, 2003, vol. 2, pp. 739–743.
12. Biswas, R., Grest, G.S., and Soukoulis, C.M., Generation of Amorphous-Silicon Structures with Use of Molecular-Dynamics Simulations, *Phys. Rev. B: Condens. Matter,* 1987, vol. 36, pp. 7437–7441.
13. Biswas, R., Bouchard, A.M., Kamitakahara, W.A., *et al.*, Vibrational Localization in Amorphous Silicon, *Phys. Rev. Lett.*, 1988, vol. 60, no. 22, pp. 2280–2283.
14. Kwon, I., Biswas, R., and Soukoulis, C.M., Molecular Dynamic Simulations of Defect Formation in Hydrogenated Amorphous Silicon, *Phys. Rev. B: Condens. Matter*, 1992, vol. 45, no. 7, pp. 3332–3339.
15. Deb, S.K., Wilding, M., Somayazulu, M., *et al.*, Pressure-Induced Amorphization and Amorphous–Amorphous Transition in Densified Porous Silicon, *Nature* (London), 2001, vol. 414, no. 6863, pp. 528–530.
16. Rothlisberger, U., Andreoni, W., and Parrinello, M., The Structure of Nanoscale Silicon Clusters, *Phys. Rev. Lett.*, 1994, vol. 72, no. 5, pp. 665–668.
17. Kobayashi, K. and Nagase, S.A., Theoretical Study of Stability of the Fullerene-Like Cage Structures of Silicon Clusters, *Bull. Chem. Soc. Jpn.*, 1993, vol. 66, pp. 3334–3338.
18. Zachariah, M.R., Carrier, M.J., and Blaisten-Barojas, E., Properties of Silicon Nanoparticles: A Molecular Dynamics Study, *J. Phys. Chem.,* 1996, vol. 100, pp. 14856–14864.
19. Stillinger, F.H. and Weber, T.A., Computer Simulation of Local Order in Condensed Phases of Silicon, *Phys. Rev. B: Condens. Matter*, 1985, vol. 31, no. 8, pp. 5262–5271.
20. Vink, R.L.C., Barkema, G.T., Van der Weg, W.F., and Mousseau, N., Fitting the Stillinger–Weber Potential to Amorphous Silicon, *J. Non-Cryst. Solids*, 2001, vol. 282, pp. 248–255.
21. Verlet, L., Computer "Experiments" on Classical Fluids: 1. Thermodynamical Properties of Lennard-Jones Molecules, *Phys. Rev.,* 1967, vol. 159, no. 1, pp. 98–103.
22. Kubicki, J.D. and Lasaga, A.C., Molecular Dynamics Simulations of SiO_2 Melt and Glass: Ionic and Covalent Models, *Am. Mineral.*, 1988, vol. 73, pp. 941–955.
23. Polukhin, V.A. and Kibanova, E.A., Molecular Dynamics Simulations of Amorphization of Carbon and Thermal Destruction of Fullerene C_{60}, *Zh. Fiz. Khim.*, 1999, vol. 73, no. 3, pp. 494–499 [*Russ. J. Phys. Chem.* (Engl. transl.), 1999, vol. 73, no. 3, pp. 421–426].
24. Wang, C.Z., Tight-Binding Molecular-Dynamics Study of Liquid Si, *Phys. Rev. B: Condens. Matter*, 1992, vol. 45, no. 21, pp. 12227–12232.